



ELSEVIER

Contents lists available at ScienceDirect

Journal of Petroleum Science and Engineering

journal homepage: www.elsevier.com/locate/petrol

An experimental study of improved oil recovery through fines-assisted waterflooding



F. Hussain^a, A. Zeinijahromi^b, P. Bedrikovetsky^b, A. Badalyan^b, T. Carageorgos^b, Y. Cinar^{a,*}

^a The University of New South Wales, Sydney, NSW, Australia

^b The University of Adelaide, Adelaide, SA, Australia

ARTICLE INFO

Article history:

Received 18 March 2013

Accepted 6 August 2013

Available online 20 August 2013

Keywords:

low salinity coreflood
fines migration
mobility control
enhanced oil recovery
relative permeability

ABSTRACT

Permeability decline during waterflooding by varying water composition, in particular with low salinity or high pH water, has been observed in numerous laboratory studies. This has been explained by the lifting, migration and subsequent plugging of pores by fine particles. Recently, mathematical models have been presented to investigate the concept of using this permeability decline for mobility control during a waterflood. Now, these models need to be tested against observations during a core flood test.

This paper presents a systematic laboratory study to investigate the underlying physics mechanisms for improved oil recovery as a consequence of injecting low-salinity water. Three sister plugs of Berea sandstone were used in the experiments. The first plug was subjected to single-phase waterflood for permeability measurements with varying salinities from 4 (high-salinity) to 0 (low-salinity) g/L NaCl. Core permeability decreased from 495 to 60 md, confirming the effect of changing water composition on permeability. The second plug saturated with high-salinity water was subjected first to primary oil flood (using Soltrol) to the connate water saturation and then to a benchmark waterflood using the same water. The oil recovery was noted and the core was restored to the connate water by a secondary oil flood. Finally, low-salinity waterflood was carried out and oil recovery was recorded. Experimental observations were interpreted using a numerical model. In order to check the reproducibility of the observations, the same experimental procedure was applied on the third plug. Results confirmed the reproducibility of the observations.

Significant decrease in water relative permeability by approximately 50% and some decrease in residual oil saturation by about 5% were observed during the low-salinity waterflood in comparison with the high-salinity waterflood. Treatment of the low-salinity coreflood data by a numerical model reveals the decrease in water relative permeability with increasing water saturation at high water saturations. This observation is explained by the expansion of rock surface exposed to low-salinity water during the increase of water saturation. The laboratory data matched by the numerical model shows a high surface exponent value ($n_A=30$), which is explained by a sharp surface area rise at high water saturations. The abnormal behavior of water relative permeability in response to low-salinity waterflood has resulted from matching water permeability increase at low water saturations and decrease at high saturations.

© 2013 Elsevier B.V. All rights reserved.

1. Introduction

Migration of reservoir fines and subsequent permeability reduction have been observed to occur in coreflood experiments as a result of decreased water salinity, increased flow velocity, water pH and temperature (Mungan, 1965; Bernard, 1967; Lever and Dawe, 1984; Khilar et al., 1990; Valdya and Fogler, 1992; Khilar and Fogler, 1998; Civan, 2007, 2010). Traditionally fines migration is considered by the oil industry to be avoided because of its detrimental effect on reservoir permeability, hence on well productivity. Numerous methods of fines immobilization by chemical treatment or nano-particle injections are presently under intensive development.

The induced reduction in the effective permeability to water in the water-swept zone, caused by fines migration during waterflooding, may potentially be used to control mobility for improving waterflood performance. Reducing the salinity of injected water is the most practical way to implement mobility control by induced fines migration. Other parameters that control the fines' release are not to be changed easily, for example, increasing flow velocity can affect the whole reservoir, not just the water-swept portion. Moreover, low salinity water is often readily available and economical compared to other alternatives.

Low-salinity waterflooding has been widely studied during last two decades. These investigations have largely focused on the effects of water salinity on wettability, relative permeability, capillary pressure and residual oil saturation (Tang and Morrow, 1999; Jerauld et al., 2008; Rivet et al., 2010; Takahashi and Kovscek, 2010). The effects appear to be separate phenomena from the movement of fines but

* Corresponding author. Tel.: +61 2 9385 5786.

E-mail address: y.cinar@unsw.edu.au (Y. Cinar).

Nomenclature

Latin letters

A	area, L^2 , m^2
A_{132}	Hamaker constant, $M L T^{-2}$, J
A_w	fraction of rock surface exposed to water
A_{wor}	fraction of rock surface exposed to water at s_{or}
c	concentration of suspended particles
D	diffusion coefficient, $L^2 T^{-1}$, $m^2 s^{-1}$
f	fractional flow of water
F_d	drag force, $M L T^{-2}$, N
F_e	electrostatic force, $M L T^{-2}$, N
F_g	gravitational force, $M L T^{-2}$, N
F_l	lifting force, $M L T^{-2}$, N
k	absolute permeability, L^2 , mD
k_o	initial absolute permeability, L^2 , mD
k_{ro}	oil relative permeability
k_{rw}	water relative permeability
l_d	lever for drag force, L, m
l_n	lever for normal force, L, m
L	core length, L, m
M	viscosity ratio
n_A	surface exponent
p	pressure, $M L^{-1} T^{-2}$, Pa
P	dimensionless pressure
s	water saturation
s_{or}	initial water saturation
s_{wi}	residual oil saturation
t	time, T, s
t_D	dimensionless time

U	overall flow velocity, $L T^{-1}$, m/s
x	linear co-ordinate, L, m
x_D	dimensionless length

Greek letters

γ	brine ionic strength, $mol L^{-3}$, and mol/l
ω	dimensionless drag constant
χ	lifting coefficient
ϕ	porosity
γ^0	ionic strength of the injected brine, $mol L^{-3}$, mol/l
ψ_{01}	surface potential of particle, mV, $M L T^{-2}$
ψ_{02}	surface potential of collector, mV, $M L T^{-2}$
ρ_o	oil density, $M L^{-3}$, kg/m^3
μ_o	oil dynamic viscosity, $M L^{-1} T^{-1}$, cp
μ_w	water dynamic viscosity, $M L^{-1} T^{-1}$, cp
β	formation damage coefficient
θ	contact angle
ε	torque ratio (erosion number)
λ_s	filtration coefficient for straining, L^{-1} , 1/m
λ	total mobility
σ	surface tension, $M T^{-2}$, N/m
σ_a	volumetric concentration of attached particles, L^{-3} , $1/m^3$
σ_{ao}	initial volumetric concentration of attached particles, L^{-3} , $1/m^3$
σ_{cr}	maximum volumetric concentration of captured particles, L^{-3} , $1/m^3$
σ_s	volumetric concentration of strained particles, L^{-3} , $1/m^3$

may occur simultaneously with fines migration. Some low salinity coreflood studies have reported the release of significant amount of fines (Bernard, 1967; Khilar et al., 1990; Tang and Morrow, 1999; Pu et al., 2010, Fogden et al., 2011) while others have reported no evidence of fines migration (Yildiz and Morrow, 1996; Jerault et al., 2008; Lager et al., 2008; Rivet et al., 2010) even though additional oil was recovered.

Pressure drop increase during low-salinity waterflooding was attributed to fines mobilization, migration, pore throat blocking and flux diversion into non-swept zones, explaining the improved microscopic displacement efficiency (Zhang and Morrow, 2006; Pu et al., 2008; Pu et al., 2010; Winoto et al., 2012). The current paper only considers the effects of fines migration and does not consider low-salinity-induced capillary phenomena. In order to separate these effects, the injections leading to fines lifting and permeability decline are called in the current work the “fines-assisted waterflooding” (Kruijsdijk et al., 2011).

The efficiency of the proposed method for the mobility control during waterflooding, as a result of fines migration in the water swept zone and the induced formation damage, has been studied by means of mathematical reservoir modeling. The Dietz-type analytical model for fines-assisted waterflooding in layer-cake reservoirs shows a significant enhancement of sweep efficiency (Lemon et al., 2011; Zeinijahromi et al., 2011). Yet, the above conclusion based on the approximate modeling must have been confirmed by a detailed 3D reservoir simulation.

The 3D mathematical model for fines-assisted waterflooding has been presented by Zeinijahromi (in press). The main assumptions are the mobilization of fines by low-salinity water due to the weakening of electrostatic forces between the particles and the rock, the migration of fine particles and the size exclusion in thin pore throats. This model gives a decrease in relative permeability to water

in response to low-salinity waterflooding. It may also result in some decrease in residual oil due to a redistribution of water flux caused by pore plugging on micro scale.

The main objective of this paper is to confirm experimentally the above-mentioned phenomenon of decline in the effective permeability to water during low-salinity coreflooding. Results of sequential corefloods with high and low salinity waters are reported in terms of the pressure drop across the core and production of oil and water. The experiments are modeled numerically using the IMPES method in order to determine the fractional flow and relative permeability from the corefloods.

2. Physics mechanisms of fines mobilization, permeability decline and improved oil recovery

A fine particle on rock surface/internal cake surface is submitted to drag (F_d), lifting (F_l), electrostatic (F_e) and gravity forces (F_g) (Fig. 1b). At the last moment of the particle lifting by the detaching forces, it rotates around the tangent point with grain. Therefore, the mechanical equilibrium of the fine particle on the surface inside the pore space is described by the balance of the torques of the above forces (Freitas and Sharma, 2001; Zinati et al., 2009; Bradford et al., 2011). Let us show that the attached particle concentration is monotonically decreasing function of the ratio between the detaching and attaching torques, which is referred to as the erosion ratio, ε ,

$$\sigma_a = \sigma_{cr}(\varepsilon), \varepsilon = \frac{(l_d/l_n)F_d(U) + F_l(U)}{F_e + F_g} \quad (1)$$

Here l_d and l_n are the levers of the drag and normal forces, respectively.¹

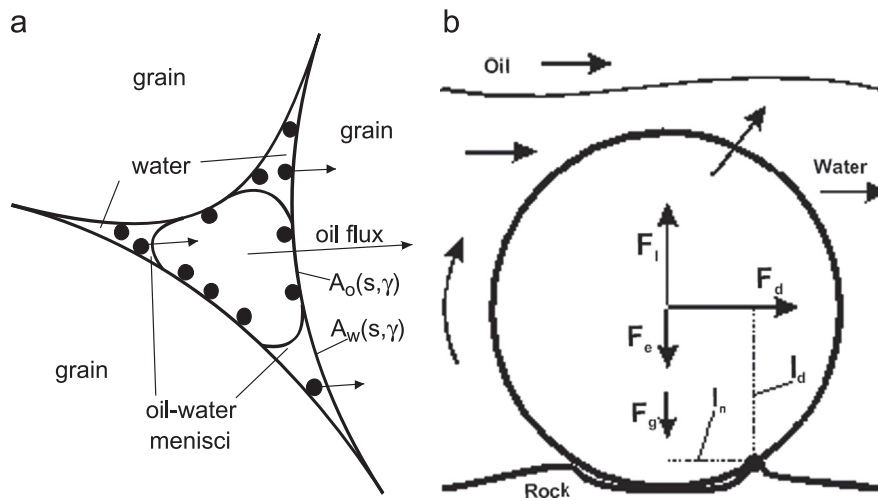


Fig. 1. Forces exerted on the attached fine particle during flow in porous media (torque balance on a single particle); (a) fine particles attached to water-wet surface and (b) torques on a fine submerged in water.

Consider a steady state of the attached particles, forming a poly-layer of particles on the pore wall. An increase in velocity increases both drag and lifting forces. The resulting increase of detaching torque cannot be equilibrated by the existing attaching torque, which is independent of velocity, see Eq. (1). Therefore, the “exceeding” upper layer of particles is mobilized. The layer thickness decreases continuously until the torque balance is achieved. So, a definite attached particle concentration corresponds to each value of the flow velocity. Similarly, the salinity decrease under a constant velocity results in a reduction in the electrostatic force and, in perturbation of the torque balance, causes the removal of the upper layer of the attached particles. For this reason, the attached particle concentration is a function of water salinity. Eq. (1) encompasses both flow velocity and brine salinity dependencies of the attached particle concentration. The detailed derivation of the so-called maximum retention function (Eq. (1)) can be found in Bedrikovetsky et al. (2011).

Increase in flow velocity/decrease in brine salinity leads to the fine particle mobilization. The detached particles migrate in porous medium until they are strained in small pores, resulting in permeability decline (Fig. 2). The corresponding permeability damage function can be obtained by keeping two terms of Taylor's expansion of the reciprocal to permeability (Pang and Sharma, 1997; Al-Abduwani et al., 2005; Civan, 2007), which is given by

$$k(\sigma_s) = \frac{k_0}{1 + \beta\sigma_s} \quad (2)$$

where σ_s is the concentration of strained fines, k is the permeability and β is the formation damage coefficient.

During displacement of oil by low-salinity water, detached particles are transported by water and block pore throats in water-invaded zones. As a result, their straining causes a decrease in effective water permeability. This has the potential to control water mobility, increasing sweep efficiency of waterflood at the reservoir scale and thereby improving oil recovery in comparison to a standard waterflood that does not induce fines migration.

3. Experimental approach

3.1. Rock sample

Berea sandstone which was known in the literature to release fines (Khilar et al., 1990) was used in the experiments. A long Berea core

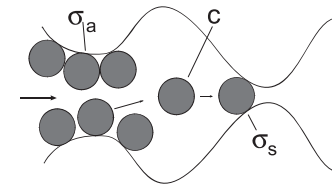


Fig. 2. Mobilized fine particles during a single phase flow are strained in thin pores resulting in permeability decrease.

was cut into three equal cylindrical plugs (2.58 cm in diameter and approximately 5.4 cm in length). First core plug was subjected to a single-phase water flow of varying salinity. The aim was to confirm the fines release and its impact on permeability. This was a precondition for the actual waterflood experiment on the second and third core plugs. The waterflood test using the third core was for the data reproducibility. The measured porosity and absolute permeability of the core plugs were approximately 23% and 495 md, respectively.

3.2. Fluids

Soltrol and distilled water/different brines of varying salinity (0.5, 2.5, 5, 10, 20, 30 and 40 g/L NaCl) were used in the experiments. The density and viscosity of both liquids were measured using a pycnometer and an Ubbelohde viscometer. The viscosities and densities are given in Table 1.

3.3. Procedure

The dry weight and dimensions of core plugs were measured. Then they were saturated with the NaCl brine of 40 g/L concentration and plug porosities were determined. Cores were then put in an oven where the temperature was kept constant at 25 °C for all experiments. The same brine was flowed through the core plug at a constant flow rate of 15 cm³/h to determine the absolute permeability. Then, two different procedures were followed:

3.3.1. Single-phase flow test

Numerous laboratory tests on sequential injection of water with decreasing salinity exhibited the permeability decline (Valdya and Fogler, 1992; Khilar and Fogler, 1998; Civan, 2007, 2010). This was explained by particle detachment and further straining (Figs. 1 and 2). Since these effects are being investigated in this study for mobility control of the displacing water during waterflooding, it was

¹ A symbol list is given at the beginning of the paper.

Table 1
Fluid properties at 25 °C and atmospheric pressure.

	Soltrol	Distilled water	NaCl brines (g/L)						
			0.5	2.5	5	10	20	30	40
Density (kg/m ³)	752	998	998	999	1001	1005	1013	1020	1028
Viscosity (mPa s)	1.4	0.88	0.88	0.89	0.90	0.92	0.95	0.97	0.99

necessary to assure before the actual oil–water displacements that the selected rock contains enough fines that can be mobilized to cause a sufficient permeability decline. The test follows the methodology described by Lever and Dawe (1984).

The first plug was subjected to a continuous single-phase waterflood with a gradual salinity decrease. The test took about 12 days for injection of eight different fluids starting with the high-salinity brine (40 g/L) and ending with the fresh water. Fig. 3 shows how the permeability decreases with the injection of less saline water. The permeability reduced first from the initial value (495 md) to a stabilized permeability of 376 md (for the high-salinity brine) and then eventually to about 60 md (for the fresh water). The stabilized permeability values were treated by the model (Eqs. (1) and (2)). Fig. 4 shows the stabilized permeability values versus the salinity. The deviations from the model can be attributed to the migration of small amount of fines released during the first waterflood.

The maximum retention function (Eq. (1)) is calculated for a bundle of parallel capillaries using the condition of the torque balance for electrostatic, drag, lifting and gravitational forces exerting on spherical particles in each pore (Bedrikovetsky et al., 2011; Lemon et al., 2011 where the expressions for the forces are presented along with a detailed derivation for the maximum retention function $\sigma_{cr}(\varepsilon)$). Below, we present the data necessary for the calculation of the forces and the maximum retention function.

The initial stabilized core permeability was 376 md with a porosity of 0.23. Using this data we calculated the parameters for log-normal pore size distribution: the pore size varies from 0.1 to 30 μm with an average size of 6.3 μm and a standard deviation of 5 μm . We assumed the monosized particles with a diameter of 1 μm . The Hamaker constant was chosen for the sandstone–kaolinite–brine system: $A_{132} = 2 \times 10^{-21}$ J (Khilar and Fogler, 1998; Israelachvili, 2006). The values of the zeta potential for different salt concentrations are presented in Table 2. We used 76 and 1193 for the drag force coefficient, ω , and the lifting force coefficient, χ , respectively.

Fig. 5 shows the results of the maximum retention function (the black curve). This was calculated using the torque balance model for parallel tubes with the log-normal distribution. The red points correspond to the values calculated from stabilized permeabilities using Eq. (2). The value of the critical salinity and the attached concentration values corresponding to high salinities were predicted fairly well. Yet, two points corresponding to low values of salinity deviate from the theoretical curve.

3.3.2. Sequential-waterflood test

This test consisted of two sequential waterfloods, first with the high-salinity water (4 g/L) and second with the low-salinity water (fresh water) in order to compare the displacement efficiency for both waterfloods. The sequence of injections was as follows. First, oil was injected to the second core until a connate water saturation (s_{wi}) was reached. Then, the high-salinity water (4 g/L) was injected to displace oil down to a residual oil saturation (s_{or}). Afterwards, oil was injected again until the same s_{wi} was achieved. Finally, fresh water was injected to the core for the low-salinity waterflood until a new s_{or} was obtained. The oil production was measured with a precision of 0.01 PV along with the pressure drop across the core with a precision

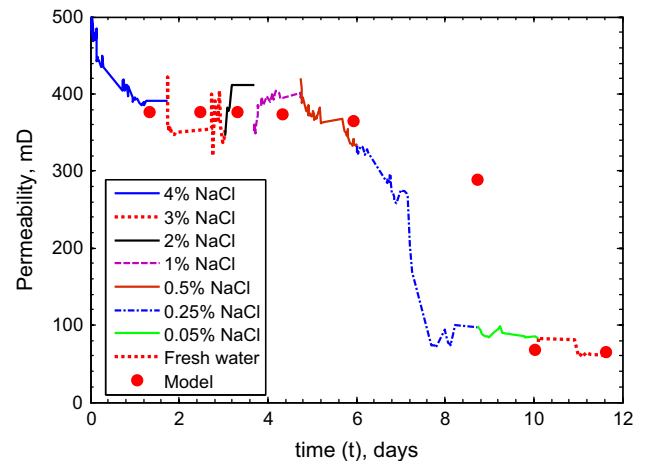


Fig. 3. Laboratory results of permeability decrease with the decrease of the injected water salinity; red points correspond to modeling data (first core plug). (For interpretation of the references to color in this figure legend, the reader is referred to the web version of this article.)

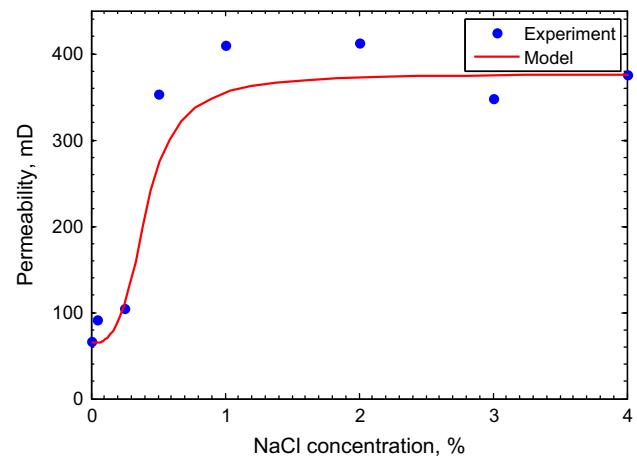


Fig. 4. Data fitting on permeability decrease during water injection with the piecewise constant decrease of salinity by the maximum retention function: stabilised experimental (blue points) and modeled (red curve) data of absolute permeability versus salinity (first core plug). (For interpretation of the references to color in this figure legend, the reader is referred to the web version of this article.)

of 225 Pa. The production and pressure drop data were used to determine phase relative permeabilities.

The material balance was used to calculate the value of s_{wi} after first and second oil injections. The pressure drop measurements were used to calculate the relative permeability to oil at s_{wi} , (k_{rowi}) after first and second oil injections. These values are very similar to each other (Table 3). This suggests that the core was saturated evenly before the high-salinity and low-salinity waterfloods.

Figs. 6 and 7 show the oil production observed during the injection of high-salinity water and fresh water, respectively. Periodic fluctuations in Figs. 6 and 7 were caused by the effluent

Table 2
Zeta potential for clay and sand for different brine concentrations.

Salt concentration (g/L)	0	0.05	0.25	0.5	1.0	2.0	3.0	4.0
Ψ_{01} (mV)	-36	-36	-36	-30	-30	-30	-30	-30
Ψ_{02} (mV)	-30	-30	-30	-20	-20	-20	-20	-20

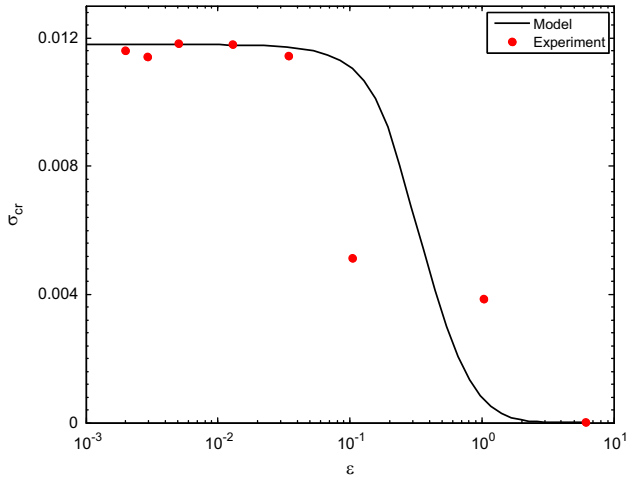


Fig. 5. Maximum retention function for the single-phase flow test with alternate salinity. The points correspond to the retention concentration values as obtained from the stabilized values of the permeability decline curve. The continuous curve corresponds to the torque-balance model (first core plug). (For interpretation of the references to color in this figure, the reader is referred to the web version of this article.)

Table 3
End-point saturation and relative permeabilities and Corey exponents.

	S_{wi}	k_{rowi}	S_{or}	k_{rwor}	n_w	n_o
High-salinity flood	0.293	0.760	0.415	0.130	3.93	2.15
Low-salinity flood	0.293	0.757	0.402	0.074	3.93	1.96

drops falling on the balance used to measure effluents' volume. Fig. 8 compares simulated recovery factors achieved during the injection of high-salinity water and fresh water. The comparison shows an incremental oil recovery by about 5% after the fresh water injection. This can be explained by decreasing the viscous fingering of water at the pore scale, which decreases the amount of the by-passed oil by water in the core plug with small scale heterogeneity. This leads to some decrease in S_{or} . The effect is similar to that of the polymer flooding where the slowed-down displacing aqueous phase results in a decrease in the capillary-trapped (by-passed) oil (Lake, 1989; Bedrikovetsky, 1993).

Figs. 9 and 10 show the pressure drop across the core during waterflooding with the high-salinity water and fresh water, respectively. Pressure drop increased during dry oil production for both injection designs. Then it decreased after water breakthrough for the high-salinity water flooding (Fig. 9). This is explained by the monotonic increase of the total mobility of two-phase fluids with the saturation increase for the values above that at the breakthrough (Lake, 1989; Bedrikovetsky, 1993).

The behavior of the pressure drop during the second stage of the fresh water injection is, however, different. Pressure drop across the core decreased during a short time period after the breakthrough and then increased monotonically. We explain this behavior by a result of two competing physics factors. On one hand, the total mobility of two-

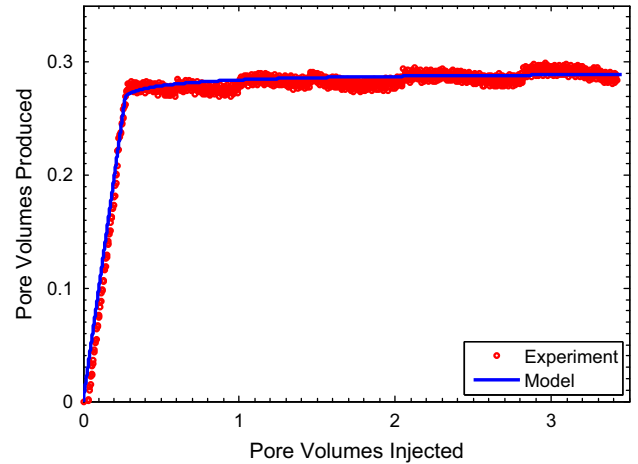


Fig. 6. PV of oil produced versus PVI for oil displacement by 4% NaCl water injection. Total produced oil (red points) is matched by the numerical model for two-phase waterflood using the Rappoport-Leas equations (second core plug). (For interpretation of the references to color in this figure legend, the reader is referred to the web version of this article.)

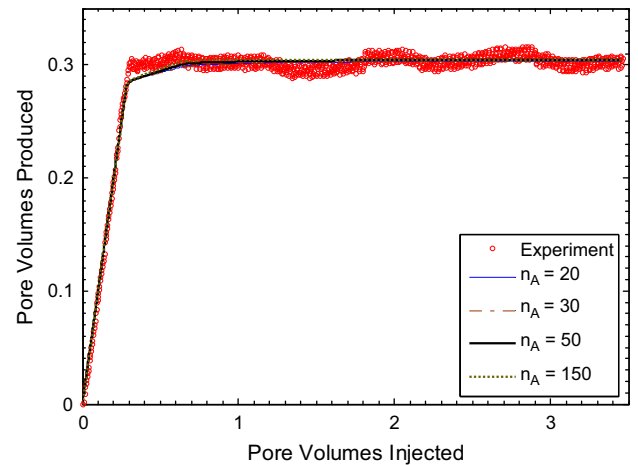


Fig. 7. PV of oil produced versus PVI for oil displacement by fresh water injection. Total produced oil (red points) is matched by the numerical model for two-phase waterflood with mobilization and migration of fines for different values of the surface exponent, n_A (second core plug). (For interpretation of the references to color in this figure legend, the reader is referred to the web version of this article.)

phase fluids increases monotonically at the absence of fines straining (see Eq. (A-7) where $\sigma_s=0$). On the other hand, the increase of water saturation causes more rock surface accessible to water (Fig. 1a). As a result, fines are released and their straining in the pores causes the induced permeability damage for the water phase (see Eq. (A-7) with $\sigma_s > 0$). This effect increases during low-salinity waterflooding and causes an increase in the pressure drop across the core at later stage (Fig. 10).

In order to demonstrate the reproducibility of the experimental observations, the same experimental procedure was followed on a sister core plug (the third core plug). Experimental results shown in Figs. 14 and 15 confirm that the observations are reproducible.

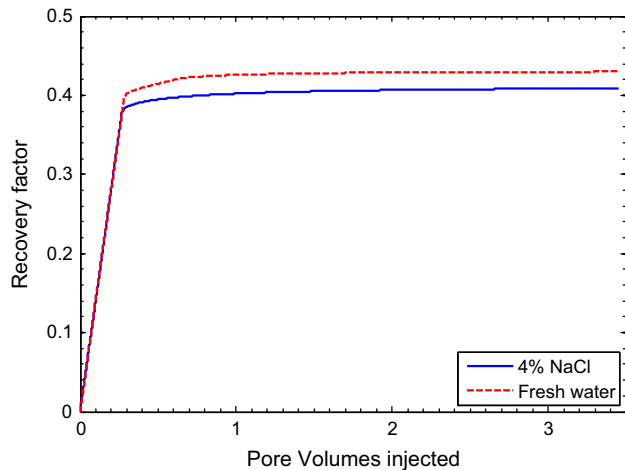


Fig. 8. Recovery factor versus PVI for oil displacement by high-salinity (4% NaCl) water and low-salinity (fresh) water. The increase in recovery factor is due to the decrease of the residual oil saturation caused by fines mobilization through low-salinity water injection. Both curves are the laboratory-matched numerical model results (second core plug).

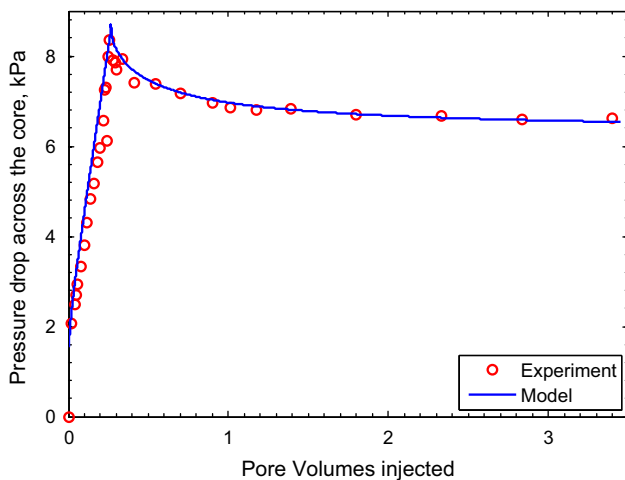


Fig. 9. Pressure drop across the core versus PVI during oil displacement by high-salinity (4% NaCl) water injection. The laboratory data (dots) is matched by the numerical Rappoport-Leas model (second core plug).

4. Determination of fractional flow curves and relative permeability from “normal” and fines-assisted waterfloods

The relative phase permeability during fines-free and fines-assisted floods was determined from production curves (Figs. 6 and 7) and pressure drop histories (Figs. 9 and 10) by matching to the numerical model.

The governing system of flow equations for oil displacement by low-salinity water is presented in Appendix A (Eqs. (A-1)–A-8). High-salinity flood corresponds to the absence of mobilized fine particles, i.e. to the case $c=0$. It transforms the system of governing equations to the traditional two-phase flow equations of Rapoport and Leas. The values of oil and water viscosities (1.4 and 1.0 cp, respectively) along with values of end point relative permeabilities indicate that the coreflood displacements performed should be stable (see Barenblatt et al., 1990; Farajzadeh and Bruining, 2011). In both cases, relative permeabilities were determined by the optimization procedure of minimizing the deviations between measured and predicted production and pressure drop.

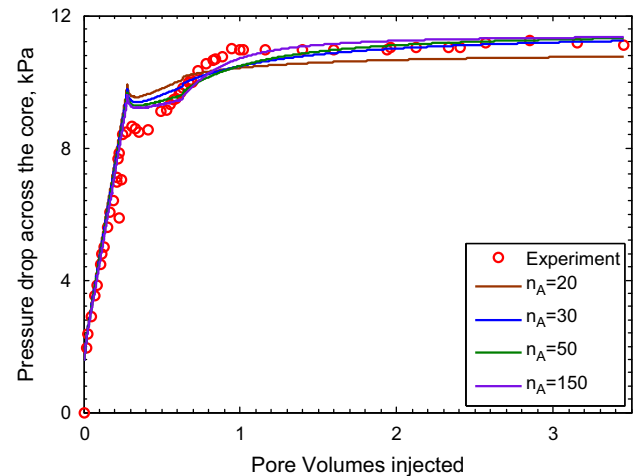


Fig. 10. Pressure drop across the core versus PVI during oil displacement by low-salinity (fresh) water. The increase in pressure drop after breakthrough is due to fines mobilization by low-salinity water injection and consequent decrease of the relative permeability to water. The data (dots) is matched by the numerical model for fines-assisted flooding accounting for capillary pressure, fines mobilization, migration, plugging and consequent water permeability decrease. Four different curves correspond to different values of the surface exponent, n_A (second core plug).

The end-point saturations were calculated from the mass balance during the creation of initial water saturation and displacement up to the residual oil. The end-point relative phase permeabilities were determined from the pressure drop across the core for the end-point saturations. So, only Corey exponents for oil and water along with Brook's parameter for capillary pressure were matched during the high-salinity-waterflood data treatment.

The same Corey's exponent was assumed for the low-salinity water as that for the high-salinity water. Brook's parameter for capillary pressure was assumed the same for both high- and low-salinity floods. The parameters tuned during the data treatment from the low-salinity water were Corey's exponent for oil, the formation damage coefficient, β , and the surface exponent, n_A .

5. Results

The raw coreflood data for oil production and pressure drop are presented in Figs. 6, 7, 9 and 10 and the results of the data treatment are shown in Figs. 11–13. The cumulative oil production and pressures drop recorded during the high-salinity waterflood (Figs. 6 and 9) were matched successfully by the numerical model for two-phase waterflood using the Rappoport-Leas equations. The cumulative oil production and pressure drop recorded during the subsequent low-salinity waterflood (Figs. 7 and 10) were matched by the numerical model for two-phase waterflood using the mathematical model developed for mobilization and migration of fines for different values of the surface exponent (n_A). As Fig. 10 shows, the match between experiments and model, especially around the breakthrough point, is not satisfactory. The reason for this mismatch is unclear which requires a repeat laboratory test.

Fig. 11 shows the blue fractional flow curve for the “normal” waterflood, which corresponds to the oil displacement by the high-salinity water in the presented laboratory tests. The red fractional flow curve in Fig. 11 corresponds to the fresh waterflood. Switching from the high-salinity water to the low-salinity water decreases the fractional flow of water. This increases the oil fractional flow, thereby resulting in an improved oil recovery.

The relative permeability to fresh water shown in Fig. 12 exhibits an unusual behavior. It starts to decrease with an increase

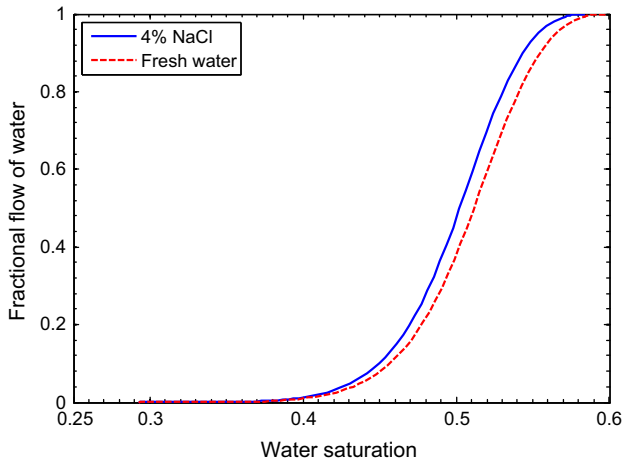


Fig. 11. Laboratory-based fractional flow curves for oil displacement by waterflooding of different salinities (second core plug). (For interpretation of the references to color in this figure, the reader is referred to the web version of this article.)

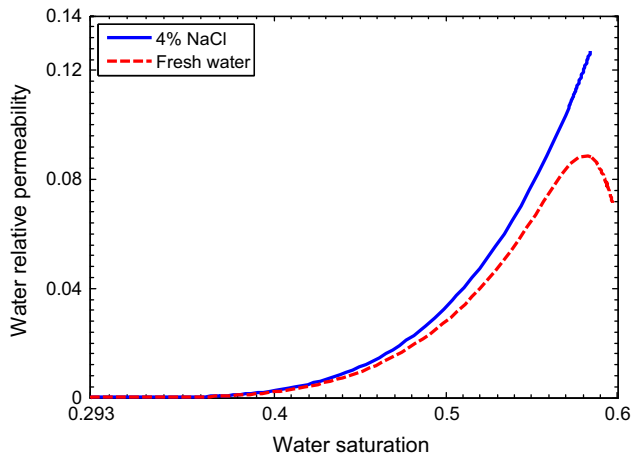


Fig. 12. Water relative permeability for the “oil/high-salinity water” and “oil/low salinity water” (second core plug). (For interpretation of the references to color in this figure, the reader is referred to the web version of this article.)

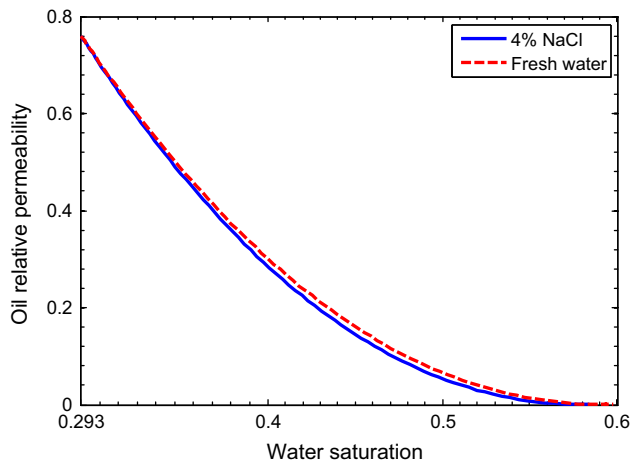


Fig. 13. Oil relative permeability for the “oil/high-salinity water” and “oil/low salinity water” (second core plug).

in water saturation. We explain this significant decrease in water relative permeability during the fines-assisted low-salinity waterflooding by the increase of the exposed rock surface to flowing

low-salinity water with an increase in water saturation. The amount of released particles increases since they are lifted from the increasing exposed surface. It causes a final decrease in water relative permeability. So, two competitive factors control the relative phase permeability to water. These are the growing water saturation that increases the water relative permeability and the increasing concentration of released and strained particles that decreases the relative permeability to water. The second factor dominates over the first under laboratory conditions during the tests and decreases the water relative permeability although water saturation keeps increasing.

The results of tuning the Corey parameters are presented in Table 3. The water-accessible-surface exponent (n_A) was obtained to be 30. Fig. 1a shows that a small increase in water saturation can cause a significant rise in water-exposed surface for large saturations. This may explain the sharp decrease in water relative permeability with the increase in saturation and the large value for the water-accessible-surface exponent, n_A .

The production curves as obtained for both high-salinity waterflood and fines-assisted flood contain very narrow intervals of continuous variations after the water breakthrough (Figs. 6 and 7). It is caused by very little oil production after the breakthrough.

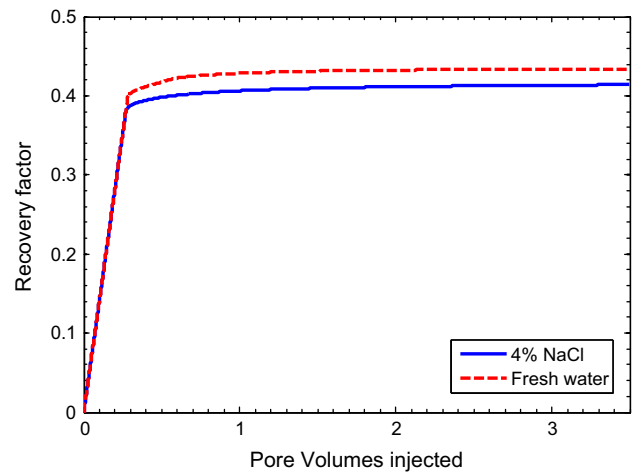


Fig. 14. Recovery factor versus PVI for oil displacement by waterflooding of different salinities. The increase in recovery factor is due to the decrease of the residual oil saturation caused by fines mobilization through low-salinity water injection. Both curves are the results of laboratory data-matched numerical models (third core plug).

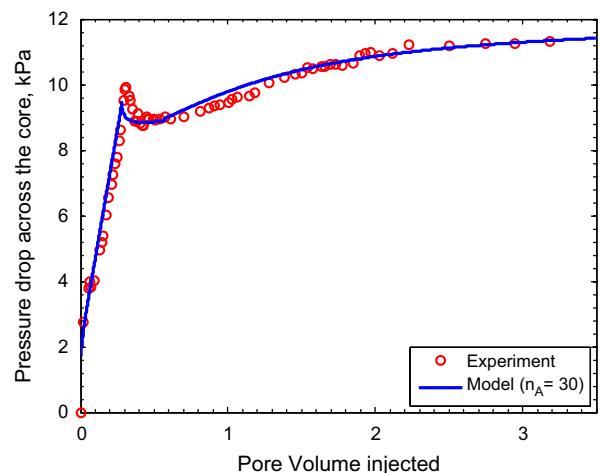


Fig. 15. Pressure drop across the core versus PVI during oil displacement by fresh water (third core plug).

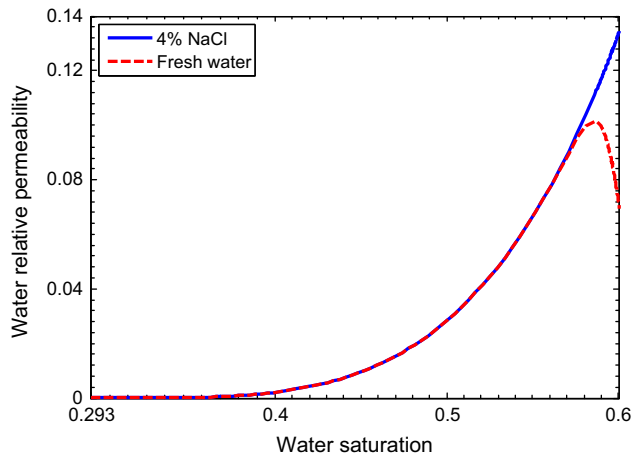


Fig. 16. Water relative permeability for the “oil/high-salinity water” and “oil/low-salinity water” as obtained by matching the results from the low salinity water (Third core plug). (For interpretation of the references to color in this figure, the reader is referred to the web version of this article.)

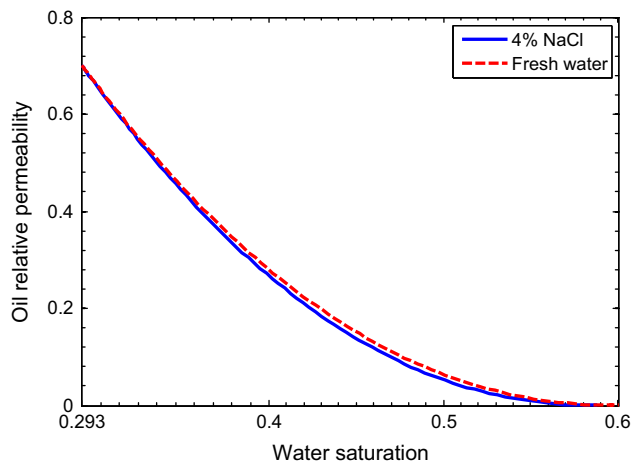


Fig. 17. Oil relative permeability for the “oil/high-salinity water” and “oil/low-salinity water” (third core plug).

Fig. 13 shows oil relative permeabilities which indicate a slight increase in oil relative permeability when fresh water was flooded compared to the normal waterflood. This is explained by some reduction in residual oil saturation as shown in the recovery plots (Fig. 8). The Corey exponent for oil, as obtained from the optimal fitting to the numerical model, decreases from 2.15 (normal waterflood) to 1.96 (fresh water flood).

With the aim to test the reproducibility of the results, the same experimental procedure was applied to a third core plug. The results shown in Figs. 14–17 confirm the same characteristics of low-salinity waterflood as observed in the test with the second core plug. The normal waterflooding test with the third core plug also exhibits the same behavior. Note especially that the match between the proposed mathematical model (with $n_A=30$) and experimental data for pressure drop is now satisfactory. This suggests that the match is very sensitive to the pressure data taken at the breakthrough time. For instance, missing out a few data points at the time of breakthrough may not display the peak in the pressure drop.

6. Discussion

The preliminary evaluation of the capacity of rocks to release fines during water injection of known composition is a single-

phase waterflood. Any fines released during single-phase waterflood provide evidence for the initial presence of in-situ fines that may potentially cause enhanced recovery during waterflooding. The above relates to fine particles attached to the water-wet fraction of rock surface.

The evaluation does not account for the fine particles attached to the oil-wet fraction of rock surface. It corresponds to clays (kaolinite, illite) that are usually oil-wet (Bennion, 2002). Yet, several laboratory tests (Berg et al., 2010; Cense et al., 2011) exhibit the alternation of clay wettability after the injection of low-salinity water that provides the access of water to attached particles. Otherwise, the clay would be covered by residual oil throughout the displacement and fines would remain attached to the rock surface.

The laboratory displacements presented here show a significant decrease in water relative permeability and some decline in residual oil in response to the application of low-salinity water injection. This is explained by the release of particles by the water phase. The results and explanations presented agree well with those reported by Muecke (1979), Sarkar and Sharma (1990), Bennion (2002) and Civan (2007 and 2010).

Pressure drop increase during low-salinity waterflooding has been repeatedly reported in the literature and attributed to permeability decrease due to pore throats plugging by mobilized fines (Zhang and Morrow, 2006; Pu et al., 2008; Pu et al., 2010; Winoto et al., 2012). Yet, the consequent alteration of phase permeability has not been discussed.

The laboratory coreflood shows a monotonic increase of pressure drop across the core during the late-time low-salinity waterflood (Fig. 10), which is different from what is usually observed during normal waterflooding (Fig. 9). Decrease of pressure drop after the breakthrough corresponds to an increase in total mobility. Water saturation increases during water injection. The two above statements suggest that total mobility increases with water saturation, resulting in monotonically increasing relative permeability to water. Fig. 9 shows pressure drop decrease after the breakthrough during normal waterflood test with the second core plug.

Appendix B presents the derivation of first and second time derivatives of pressure drop (see Eqs. (B-7) and B-8)). Eq. (B-7) shows that total mobility is positive if the slope of the pressure drop curve does not exceed the tangent of straight line connecting points $(t_D, \Delta P(t_D))$ and $(0,0)$. Pressure drop curves from corefloods of second and third core sections, shown in Figs. 9, 10 and 15, meet this condition. As it follows from (B-8), the sign of s -derivative of total mobility is the same as that for second t_D -derivative of pressure drop across the core. Concave pressure drop curves are obtained from high-salinity waterflooding tests (Fig. 9), upon which total mobility exhibits monotonically increasing behavior after the breakthrough. Relative permeability to oil decreases monotonically, so relative permeability to water increases. For convex pressure drop curves as obtained from low salinity waterflooding tests for the late stage of injection (Figs. 10 and 15), total mobility monotonically decreases (Eq. (B-8)). Usually the derivative of oil relative permeability is zero at residual oil saturation, since the Corey power for oil exceeds unity. Therefore, the s -derivative of relative permeability to water at residual oil saturation is negative. So, it is also negative in some neighborhood of point $s=1-s_{or}$. Indeed, relative permeability curves to water as obtained from fresh water injections into second and third core plugs (the red curves in Figs. 12 and 16) show decrease of water relative permeability tending to the residual oil saturation.

The laboratory coreflooding presented in this work does not fulfill the conditions of large scale approximation: the value of capillary-viscous ratio is 21 while it must be significantly lower than one in order to neglect the effects of capillary forces. Therefore, the JBN

method is not applicable to the presented core flood tests. So, the calculations of relative permeability were performed using a numerical model for Eqs. (A-1–A-7).

The effect of water permeability reduction is explained by the increase of the fraction of rock surface, accessible to moving water, during water injection – fine particles are released from the expanding water exposed surface, causing an increase in permeability damage (Fig. 1a).

A remarkably high value for the exponent of the surface area accessible to moving water ($n_A=30$ in Eq. (A-8)) is obtained from matching the coreflood data by the numerical model. This can be explained by the high increase of the rock surface exposed to water at high water saturations. Fig. 1a shows that it occurs where the area accessible to mobile oil tends to zero, which corresponds to a water–oil menisci tangent to the rock surface at some high water saturation $s=s_1$. It means that the derivative dA_w/ds tends to infinity at this saturation value. All functions with singularity $(s-s_1)^{-n}$ in Eq. (A-8) approximate this behavior for large n values. In our case, a good match is achieved with $n_A=20$, further increase of the exponent n does not improve the approximation. This is the reason of low sensitivity of the model to the surface exponent, shown in Figs. 7 and 10.

The conclusions support the idea of using induced fines migration and consequent formation damage to water for mobility control during waterflooding. Yet, further laboratory investigation of fines-assisted waterflooding is required in order to identify the oil–water–rock conditions favorable for fines-assisted waterflooding and verify the mathematical model developed. High accuracy measurements of the fine particle concentration in the produced water would allow the determination of the maximum retention function under two-phase flow. It would also permit interpreting the fines release dynamics with respect to the increase of the water cut and the fraction of the rock area exposed to water. The accurate monitoring of the fine particle concentration in the produced water was not made in the tests reported here. Monitoring of the produced water salinity would allow more accurate prediction of the low salinity water breakthrough. It would also permit its correlation with the fines release. In the present tests, the effluent salinity was not monitored. Chemical and mineralogical analysis of the produced fines and of the originally in-situ fines would allow assuring the above claimed mechanisms.

The improved oil recovery mechanism of fines-assisted waterflood by inducing the formation damage into the water swept area is different from that of improved relative permeability and capillary pressure during low salinity waterflood. Although the above can occur simultaneously, the geological conditions for fines migration and for capillary phenomena alternation are different. Fines migration may occur in rocks with high contents of kaolinite or illite clays (Lever and Dawe, 1984; Bennion, 2002), while capillary phenomena changes depend on rock mineralogy and oil properties (Yildiz and Morrow, 1996; Morrow and Buckley, 2011). Capillary effects appear to be a separate phenomenon from fines-induced formation damage in the water phase. Some low-salinity coreflood studies have reported the release of significant amounts of fines (Bernard 1967; Tang and Morrow 1999; Pu et al. 2010; Fogden et al. 2011), while others presented no evidence of fines migration (Yildiz and Morrow 1996; Jerauld et al. 2008; Lager et al. 2008; Rivet et al. 2010), even though additional oil was recovered.

This work presents a comparison between the “normal” and fines-assisted waterfloods for a strongly water-wet rock. Further studies for oil-wet and mixed-wet rocks are required. In particular, the mechanism of oil-wet and partly-wet fines mobilization by advancing water–oil menisci was proposed by Tang and Morrow (1999) and observed by Fogden et al. (2011). This mechanism must be included in the mathematical model and be considered together with the abovementioned mechanism of fines release by low-salinity waterflood after passing the displacement front.

More detailed laboratory analysis of produced water and rock is required to validate the mathematical model for fines-assisted waterflooding.

7. Conclusions

A laboratory investigation of fines-free and fines-assisted waterflooding and data interpretation by the numerical one-dimensional model have been presented. The following conclusions are drawn: (1) Single-phase test with decreasing salinity showed that the tested Berea core had potential for fines release and the consequent permeability decline by the flooding with low salinity water. (2) The injection of fresh water reduced the residual oil saturation by about 5% and the water relative permeability by approximately 50%. The reproducibility of these results was confirmed by a second test on a sister plug. (3) Treatment of the coreflood data by the numerical model reveals the decrease in water relative permeability during the increase of water saturation for high water saturations. This observation is explained by the expansion of the rock surface exposed to water during the increase of water saturation. (4) The laboratory data fitting by the numerical model shows a high surface exponent value ($n_A=30$), which is explained by a sharp surface area rise at high water saturations.

Acknowledgments

The work is sponsored by ARC Discovery and ARC Linkage grants. Authors thank T. Rodrigues, I. Abbasy, K. Boyle (Santos Ltd., Australia) and F. Machado, A.L.S. de Souza, C.A. Furtado (Petrobras, Brazil) for detailed discussions of the field applications, for support and encouragement. PB is grateful to Prof. P. Currie (Delft University of Technology) and Prof. A. Shapiro (Technical University of Denmark) for long-time co-operation in formation damage. Especial thanks are due to Shell Research colleagues Prof. Cor Van Kruijsdijk, Prof. J. Bruining, Dr. Farahzadeh, Dr. G. Glasbergen and Dr. Mahani for fruitful discussions and the term “fines-assisted waterflooding”. Especial thanks are due to Prof. H. Bruining for providing a numerical code for solution of the Rappoport–Leas equations.

Appendix A. Core-scale mathematical model for fines-assisted waterflood

Full governing system for two-phase flow with lifting, migration and straining of fine particles in the water phase consists of equations for the volumetric balance of the overall two-phase flux of incompressible phases

$$\nabla(U) = 0 \quad (\text{A-1})$$

the volumetric balance of water, where f is a fractional flow for water and P_c is the capillary pressure between two phases

$$\frac{\partial[(\phi - \sigma_a - \sigma_s)S]}{\partial t} + U \nabla f(s, \sigma_s) = - \frac{k \sigma_{wo} \cos \theta \nabla \left(\frac{f k_{ro}(s)}{\mu_o} \nabla J(s) \right)}{\sqrt{k/\phi}} \quad (\text{A-2})$$

$$f(s, \sigma_s) = \left[1 + \frac{k_{ro}(s) \mu_w (1 + \beta \sigma_s)}{k_{rw}(s) \mu_o} \right]^{-1}, \quad P_c(s) = \frac{\sigma_{wo} \cos \theta}{\sqrt{k/\phi}} J(s)$$

the mass balance for suspended, attached and strained particles

$$\frac{\partial}{\partial t} [(\phi - \sigma_a - \sigma_s) S c + \sigma_a + \sigma_s] + U \nabla (c f) = - \frac{k \sigma_{wo} \cos \theta \nabla \left(\frac{f k_{ro}(s)}{\mu_o} \nabla J(s) \right) - \nabla (D_s \nabla c)}{\sqrt{k/\phi}} \quad (\text{A-3})$$

the maximum retention function, i.e. dependency of the maximum attached particle concentration of erosion number, saturation and

water phase velocity

$$\sigma_a(U_w, \gamma, s) = \frac{\sigma_{cr}(U_w, \gamma)A_w(s, \gamma) + \sigma_{a0}[A - A_w(s, \gamma)]}{A}$$

$$U_w = (Uf(s, \sigma_s)) / (s(\phi - \sigma_a - \sigma_s)) \quad (\text{A-4})$$

the kinetics of fine particles straining

$$\frac{\partial \sigma_s}{\partial t} = \lambda_s c U \frac{f}{s} \quad (\text{A-5})$$

the mass balance of salt

$$\frac{\partial}{\partial t}[(\phi - \sigma_a - \sigma_s)s\gamma] + \nabla[\gamma f(s, \sigma_s)U]$$

$$= -\frac{k\sigma_{wo} \cos \theta}{\sqrt{k/\phi}} \nabla \left(\gamma \frac{f k_{ro}(s)}{\mu_o} \nabla J(s) \right) - \nabla(Ds \nabla \gamma) \quad (\text{A-6})$$

and modified Darcy's law for two-phase flow accounting for water phase reduction due to fines straining

$$U = -k \left[\frac{k_{rw}(s)}{\mu_w(1 + \beta\sigma_s)} + \frac{k_{ro}(s)}{\mu_o} \right] \nabla p \quad (\text{A-7})$$

Eq. (A-1)–(A-7) is the modification of the traditional equations of two-phase incompressible flow with capillary pressure (see Lake, 1989; Bedrikovetsky, 1993). Here Eq. (A-2) accounts for the porosity defect due to the attached and retained fine particles; the expression for fractional flow curve contains the formation damage factor of water permeability reduction due to the strained fines (see Bedrikovetsky et al., 2011). Eq. (A-3) expresses fines transport by advective, capillary and diffusive fluxes.

It is assumed that the maximum retention function for a single phase flow, $\sigma_{cr}(U, \gamma)$ is known and that for two-phase flow (A-4) is the total of the initial attached fines concentration on the oil-wet surface and the critical attached fines concentration on the water-wet surface. By analogy with Corey's formulae, the following expression for the water-wet fraction of the rock surface is assumed

$$A_w(s, \gamma) = A_{wor} \left(\frac{s - s_{wi}}{1 - s_{wi} - s_{or}} \right)^{n_A} \quad (\text{A-8})$$

where n_A is the surface exponent. It corresponds to the assumption that overall water phase is mobile above the threshold saturation, i.e. the attached fines are dragged by the moving water from the overall water-wet surface (Bennion, 2002).

Eq. (A-5), for straining kinetics, contains velocity of water phase since straining occurs in the water-filled fraction of pore space. Eq. (A-6), for solute transport, expresses salt transfer by advective, capillary and diffusive fluxes. Eq. (A-7) contains the formation damage factor of water permeability reduction due to strained fines.

Eqs. (A-1)–(A-7) can be significantly simplified for a large reservoir length scale. Yet, it describes the fines-assisted waterflooding at the core scale. Therefore, it was used in the current work to determine relative phase permeability for high salinity and low salinity water floods from the laboratory data.

The IMPES numerical method was used to solve the Rapport-Leas Eqs. (A-1), (A-2), and (A-7) for high salinity waterflood without fines, where $c=0$. The code was modified for waterflood with fines to account for fines release, straining and consequent permeability damage to the water phase behind the salinity front.

Appendix B. Relationship between trends of pressure drop and total mobility

Let us show that the relative permeability to water, as determined from corefloods where pressure drop across the core after

the breakthrough is a monotonically increasing convex curve, is non-monotonic.

Discuss large scale approximation of the system ((A-1)–(A-7))

$$\frac{\sigma \cos \theta \sqrt{k\phi}}{\mu_o UL} \ll 1, \quad \lambda_s L \gg 1, \quad \frac{D}{UL} \ll 1$$

corresponding to the small ratio of capillary to viscous forces, short capture-free particle run and large Peclet number in “long” cores (Barenblatt et al., 1990).

A-The asymptotic form of Eqs. (A-1)–(A-7) is a hyperbolic 2×2 system of conservation laws for water and for salt concentration (Zeinijahromi, in press). The solution of 1D displacement problem corresponding to low salinity water injection is self-similar (Bedrikovetsky, 1993).

$$s(x_D, t_D) = S(\xi), \quad \gamma(x_D, t_D) = \gamma(\xi), \quad \xi = x_D/t_D \quad (\text{B-1})$$

where the following dimensionless parameters for system (A-1)–(A-7) are used

$$x_D = \frac{x}{L}, \quad t_D = \frac{Ut}{\phi L}, \quad P = \frac{kp}{\mu_o UL}, \quad \Delta P = P(1, t_D) - P(0, t_D) \quad (\text{B-2})$$

The derivations below do not use the solution but only its self-similarity.

Darcy's law for two-phase flux (A-7) in dimensionless coordinates becomes

$$1 = -\lambda(s) \frac{\partial P}{\partial x_D}, \quad \lambda(s) = Mk_{rw}(s, \gamma) + k_{ro}(s, \gamma) \quad (\text{B-3})$$

Expressing the pressure gradient (B-3) and integrating in x_D from 0 to 1 yields the expression for pressure drop across the core:

$$\Delta P = \int_0^1 \frac{dx_D}{\lambda(s(x_D, t_D))} \quad (\text{B-4})$$

Changing the integration variable in (B-4) from x_D to ξ results in

$$\Delta P = t_D \int_0^{1/t_D} \frac{d\xi}{\lambda(s(\xi))} \quad (\text{B-5})$$

Expressing the integral from (B-5) and taking its ξ -derivative yields

$$\frac{1}{\lambda(s(1/t_D))} = \frac{d}{d\xi} [\Delta P(\xi)\xi], \quad \xi = 1/t_D \quad (\text{B-6})$$

Here, $x_D=1$ at the core outlet.

Applying the chain rule for the derivative in $t_D=1/\xi$ in (B-6) yields the JBN's expression for the total mobility of two-phase fluid (see Johnson et al., 1959):

$$\frac{1}{\lambda(s(1/t_D))} = \Delta P(t_D) - t_D \frac{d[\Delta P(t_D)]}{dt_D} \quad (\text{B-7})$$

Taking t_D -derivative from both sides of Eq. (B-7) yields

$$\frac{1}{\lambda^2(s, \gamma)} \frac{\partial \lambda(s, \gamma)}{\partial s} \frac{ds(1, t_D)}{dt} = t_D \frac{d^2[\Delta P(t_D)]}{dt_D^2} \quad (\text{B-8})$$

Since the total mobility, $\lambda(s, \gamma)$ is positive and the outlet water saturation is monotonically increasing function during water injection, sign of the left hand side of Eq. (B-8) coincides with the sign of the s -derivative of the total mobility. So, the sign of the s -derivative of total mobility is the same as that for the second t_D -derivative of pressure drop across the core.

References

- Al-Abduwani, F., Farajzadeh, R., van den Broek, W., Currie, P., Zitha, P., 2005. Filtration of micron-sized particles in granular media revealed by X-Ray computed tomography. *Rev. Sci. Instrum.* 76 (10) (103704-1–103704-6).
- Barenblatt, G.I., Entov, V.M., Ryzhik, V.M., 1990. *Theory of Fluid Flows Through Natural Rocks*. Kluwer Academic Publishers, Dordrecht, Boston, London.
- Bedrikovetsky, P., 1993. Mathematical theory of oil and gas recovery; with applications to ex-USSR oil and gas fields. In: Rowan, G. (Ed.), *Petroleum Engineering and Development Studies*, vol. 4. Kluwer Academic Publishers, Dordrecht, The Netherlands. (trans. R. Loshak).
- Bedrikovetsky, P., Siqueira, F., Furtado, C., Souza, A., 2011. Modified particle detachment model for colloidal transport in porous media. *Transp. Porous Media* 86 (2), 353–383, <http://dx.doi.org/10.1007/s11242-010-9626-4>.
- Bennion, D.B., 2002. An overview of formation damage mechanisms causing a reduction in the productivity and injectivity of oil and gas producing formations. *J. Can. Pet. Technol.* 41 (11), 29–36, <http://dx.doi.org/10.2118/02-11-das>.
- Berg, S., Cense, A.W., Jansen, E., Bakker, K., 2010. Direct experimental evidence of wettability modification by low salinity. *Petrophysics* 52 (5), 314–322 (doi:2010.v51n5a3).
- Bernard, G.G., 1967. Effect of floodwater salinity on recovery of oil from cores containing clays. In: Paper SPE 1725 Presented at the SPE California Regional Meeting, 26–27 October. Los Angeles, California, USA.
- Bradford, S.A., Torckaban, S., Simunek, J., 2011. Modeling colloid transport and retention in saturated porous media under unfavorable attachment conditions. *Water Resour. Res.* 47 (10), W10503, <http://dx.doi.org/10.1029/2011wr010812>.
- Cense, A.W., Berg, S., Bakker, K., Jansen, E., 2011. Direct visualization of designer water flooding in model experiments. In: Paper SPE-144936-MS Presented at the SPE EOR Conference, 19–21 July. Kuala Lumpur, Malaysia.
- Civan, F., 2007. *Reservoir Formation Damage: Fundamentals, Modeling, Assessment, and Mitigation*. Gulf Professional Publishing, Elsevier, Burlington.
- Civan, F., 2010. Non-isothermal permeability impairment by fines migration and deposition in porous media including dispersive transport. *Transp. Porous Media* 85 (1), 233–258, <http://dx.doi.org/10.1007/s11242-010-9557-0>.
- Farajzadeh, R., Bruining, J., 2011. An analytical method for predicting the performance of gravitationally-unstable flow in porous media. In: Paper SPE-143420-MS Presented at the SPE EUROPEC/EAGE Annual Conference and Exhibition, 23–26 May. Vienna, Austria.
- Freitas, A., Sharma, M., 2001. Detachment of particles from surfaces: an Afm study. *J. Colloid Interface Sci.* 233 (1), 73–82, <http://dx.doi.org/10.1006/jcis.2000.7218>.
- Fogden, A., Kumar, M., Morrow, N.R., Buckley, J.S., 2011. Mobilization of fine particles during flooding of sandstones and possible relations to enhanced oil recovery. *Energy Fuels* 25 (4), 1605–1616, <http://dx.doi.org/10.1021/ef101572n>.
- Israelachvili, J.N., 2006. *Intermolecular and Surface Forces*. Academic Press, London.
- Jerauld, G., Webb, K., Lin, C., Seccombe, J., 2008. Modeling low-salinity waterflooding. *SPE Reserv. Eval. Eng.* 11 (6), 1000–1012, <http://dx.doi.org/10.2118/102239-PA>.
- Johnson, E., Bossler, D., Naumann, V., 1959. Calculation of relative permeability from displacement experiments. *Trans. AIME* 216, 370–372.
- Khilar, C.K., Vaidya, R.N., Fogler, H.S., 1990. Colloidally-induced fines release in porous media. *J. Pet. Sci. Eng.* 4, 213–221.
- Khilar, K., Fogler, H., 1998. *Migrations of Fines in Porous Media*. Kluwer Academic Publishers, Dordrecht/London/Boston.
- Van Kruijsdijk, C.P.J.W., Mahani, H., 2011. Shell Research. Rijswijk, The Netherlands, Personal communication.
- Lager, A., Webb, K.J., Black, C.J.J., Singleton, M., Sorbie, K.S., 2008. Low salinity oil recovery—an experimental investigation. *Petrophysics* 49 (1), 28–35 (doi:2008-v49n1a2).
- Lake, L., 1989. *Enhanced Oil Recovery*. Prentice-Hall, New Jersey.
- Lemon, P., Zeinijahromi, A., Bedrikovetsky, P., Shahin, I., 2011. Effects of injected-water salinity on waterflood sweep efficiency through induced fines migration. *J. Can. Pet. Technol.* 50 (9), 82–94, <http://dx.doi.org/10.2118/140141-pa>.
- Lever, A., Dawe, R., 1984. Water-sensitivity and migration of fines in the hopeman sandstone. *J. Pet. Geol.* 7 (1), 97–107, <http://dx.doi.org/10.1111/j.1747-5457.1984.tb00165.x>.
- Morrow, Buckley, 2011. Improved oil recovery by low-salinity waterflooding. *J. Pet. Technol.* 63 (4), 106–113.
- Muecke, T.W., 1979. Formation fines and factors controlling their movement in porous media. *J. Pet. Technol.* 31 (2), 144–150, <http://dx.doi.org/10.2118/7007-pa>.
- Mungan, N., 1965. Permeability reduction through changes in pH and salinity. *J. Pet. Technol.* 17 (12), 1449–1453, <http://dx.doi.org/10.2118/1283-PA>.
- Pang, S., Sharma, M.M., 1997. A model for predicting injectivity decline in water-injection wells. *SPE Form. Eval.* 12 (3), 194–201, <http://dx.doi.org/10.2118/28489-PA>.
- Pu, H., Xie, X., Yin, P., Morrow, N., 2008. Application of coal bed methane water to oil recovery by low salinity waterflooding. In: SPE paper 113410 Presented at SPE EOR Symposium. Tulsa.
- Pu, H., Xie, X., Yin, P., Morrow, N., 2010. Low-salinity waterflooding and mineral dissolution. In: Paper SPE Paper 134297 Presented at the SPE Annual Technical Conference and Exhibition, 19–22 September. Florence, Italy.
- Rivet, S., Lake, L., Pope, G., 2010. A coreflood investigation of low-salinity enhanced oil recovery. In: Paper SPE Paper 134297 Presented at the SPE Annual Technical Conference and Exhibition, 19–22 September. Florence, Italy.
- Sarkar, A., Sharma, M., 1990. Fines migration in two-phase flow. *J. Pet. Technol.* 42 (5), 646–652, <http://dx.doi.org/10.2118/17437-PA>.
- Takahashi, S., Kovscek, A.R., 2010. Wettability estimation of low-permeability, siliceous shale using surface forces. *J. Pet. Sci. Eng.* 75 (1–2), 33–43, <http://dx.doi.org/10.1016/j.petrol.2010.10.008>.
- Tang, G., Morrow, N., 1999. Influence of brine composition and fines migration on crude oil/brine/rock interactions and oil recovery. *J. Pet. Sci. Eng.* 24 (2–4), 99–111, [http://dx.doi.org/10.1016/S0920-4105\(99\)00034-0](http://dx.doi.org/10.1016/S0920-4105(99)00034-0).
- Valdya, R., Fogler, H., 1992. Fines migration and formation damage: influence of pH and ion exchange. *SPE Prod. Eng.* 7 (4), 325–330, <http://dx.doi.org/10.2118/19413-PA>.
- Winoto, W., Loahardjo, N.N., Xie, X., Yin, P., Morrow, N., 2012. Secondary and tertiary recovery of crude oil from outcrop and reservoir rocks by low salinity waterflooding. In: SPE Paper 154209 Presented at Eighteen SPE Improved Oil Recovery Symposium held in Tulsa, OK, USA, 14–18 April.
- Yildiz, H., Morrow, N., 1996. Effect of brine composition on recovery of moutray crude oil by waterflooding. *J. Pet. Sci. Eng.* 14 (3–4), 159–168, [http://dx.doi.org/10.1016/0920-4105\(95\)00041-0](http://dx.doi.org/10.1016/0920-4105(95)00041-0).
- Zeinijahromi, A., Lemon, P., Bedrikovetsky, P., 2011. Effects of induced migration of fines on water cut during waterflooding. *J. Pet. Sci. Eng.* 78, 609–617.
- Zeinijahromi, A., Phuong, Thi Nguyen, Bedrikovetsky, P., 2013. Mathematical model for fines migration assisted waterflooding with induced formation damage. *Journal of Society of Petroleum Engineers SPEJ.* (in press).
- Zhang, Y., Morrow, N., 2006. Comparison of secondary and tertiary recovery with change in injection brine composition for crude oil/sandstone combinations. In: SPE Paper 99757 Presented at the 2006 SPE/DOE Symposium on Improved Oil Recovery held in Tulsa, OK, 22–26 April.
- Zinati, F.F., Farajzadeh, R., Currie, P., Zitha, P., 2009. Modeling of external filter cake build-up in radial geometry. *Pet. Sci. Technol.* 27 (7), 746–763.